Supporting Information

Monophenyl-Featured Side-Chain-Random Terpolymer Achieving Organic Solar Cells with Efficiency Beyond 19%

Deng Zhou, Lingchen Kong, Lianjie Zhang, Jiafeng Zhang, Mingqing Chen, Xinkang Wang, Xunchang Wang, Dongge Ma, Renqiang Yang*, and Junwu Chen**

D. Zhou, L. Kong, Dr. L. Zhang*, J. Zhang, M. Chen, X. Wang, Prof. D. Ma, Prof. J. Chen*

Institute of Polymer Optoelectronic Materials & Devices

Guangdong Basic Research Center of Excellence for Energy & Information Polymer Materials

State Key Laboratory of Luminescent Materials & Devices

South China University of Technology

Guangzhou 510640, P. R. China.

E-mail: lianjiezhang@scut.edu.cn; psjwchen@scut.edu.cn

Dr. X. Wang, Prof. R. Yang*

Key Laboratory of Optoelectronic Chemical Materials and Devices (Ministry of Education)

School of Optoelectronic Materials & Technology

Jianghan University

Wuhan 430056, China

E-mail: yangrq@jhun.edu.cn

Experimental Section

Materials

All reagents and solvents were purchased from commercial sources (like *J&K*, Energy Chemical, Derthon, and Acros) and used without further purification unless otherwise specified. All manipulations involving air-sensitive reagents were performed under an atmosphere of dry argon.

Device Fabrication and Characterization:

The device structure was ITO/PEDOT:PSS/Donor:Acceptor/PNDITF3N-Br/Ag. The ITO-coated glass was preclean and modified by a thin layer of PEDOT:PSS at 3000 rpm for 20 s, and then dried at 150 ℃ for 15 min in air. The thickness of the PEDOT: PSS layer is ~30 nm. After the blend solution of the active layers were spin-coated onto the ITO substrate, the electron-transport layer of PNDIT-F3N-Br (~5 nm) was spin-coated on top of the active layers. Then, those samples were brought into an evaporating chamber and a 100 nm thick silver layer was thermally evaporated on the PNDIT-F3N-Br layer at a base pressure of 1×10^{-4} mbar. The active area of each device was 4 mm^2, defined by a shadow mask.

The fabrication details for the PhEH10:Y6-BO, PhEH10:BTP-eC9, PhEH10:L8-BO, and PhEH10:L8-BO: BTP-eC9 based OSCs are depicted. For PhEH10:Y6-BO based devices, the PhEH10:Y6-BO ratio was kept at 1:1.2 (w/w) with the donor concentration of 7.5 mg/mL in chloroform. A 75% weight ratio of 1-chloro-4-iodobenzene (CIB) relative to donor and acceptor was employed. Thermal annealing (TA) process was carried out at 100 ℃ for 3 min. For the PhEH10: BTP-eC9 based devices, the PhEH10:BTP-eC9 ratio was kept at 1:1.2 (w/w) with the donor concentration of 7 mg/mL in chloroform. A 75% weight ratio of 1-chloro-4-iodobenzene (CIB) relative to donor and acceptor was employed. The TA process was carried out at 100 ℃ for 3 min. For the PhEH10:L8-BO based devices, the PhEH10:L8-BO ratio was kept at 1:1.2 (w/w) with the donor concentration of 7.5 mg/mL in chloroform. A 75% weight ratio of 1-chloro-4-iodobenzene (CIB) relative to donor and acceptor was employed. The TA process was carried out at 100 ℃ for 3 min. And for the PhEH10:L8-BO: BTP-eC9 based devices, the PhEH10:L8-BO: BTP-eC9 ratio was kept at 1:1:0.2 (w/w) with the donor concentration of 7.5 mg/mL in chloroform. A 75% weight ratio of 1-chloro-4-iodobenzene (CIB) relative to donor and acceptor was employed. The TA process was carried out at 80 ℃ for 3 min.

Instruments and characterization

The PCE was determined from *J-V* curve measurements (using a Keithley 2400 source meter) under a 1 sun, AM 1.5G spectrum from a solar simulator (Oriel model 91192; 1000 W m^{-2}). All the masked and unmasked tests gave consistent results with relative errors within 5%. The solar simulator illumination intensity was determined using a monocrystal silicon reference cell (Enli/SRC2020, with KG-5 visible color filter) calibrated by the National Renewable Energy Laboratory (NREL). The calculated J_{sc} values obtained by integrating the product of the EQE with the AM 1.5G solar spectrum agreed with the measured value to within 5%.

TPC and TPV Measurements: The transient photocurrent and transient photovoltage characteristics of devices were measured by applying 500 nm laser pulses with a pulse width of 120 fs and a low pulse energy to the short-circuit devices in the dark. The laser pulses were generated from an optical parametric amplifier (TOPAS-Prime) pumped by a mode-locked Ti: sapphire oscillator seeded regenerative amplifier with a pulse energy of 1.3 mJ at 800 nm and a repetition rate of 1Hz (spectra Physics Spitfire Ace). The charge extraction time was extracted from the fitting line of the TPC signal with the equation of $\Delta I = A\exp(t/T)$, where A is a constant that fits the peak height, t is time, and T is the charge extraction time. The transient photovoltage was tested under the open-circuit condition to explore the photovoltage decay. The photovoltage decay kinetics of all devices follow a mono-exponential decay of $\Delta V = A\exp(-t/T)$, where A is a constant that fits the peak height, t is the time, and T is the charge carrier lifetime.

Morphology characterizations: The atom force microscopy (AFM) images were tested by a Nano Scope NS3A system (Digital Instrument) to observe the surface morphology of active layers.

The grazing incidence wide-angle X-ray scattering (GIWAXS) experiments were conducted using the XEUSS SAXS/WAXS equipment. d-Spacing distance is obtained by $2\pi/q$, and CCL was calculated by Scherrer equation of $CCL = 2\pi K/FWHM$, where K is shape factor (0.93 is used here), FWHM represents the full-width at half-maximum of the peak.

Hole-only and electron-only devices were fabricated to measure the hole and electron mobilities of active layers using the space charge limited current (SCLC) method with the hole-only device of ITO/PEDOT:PSS/active layer/MoO_3/Ag and electron-only device of ITO/ZnO/PNDIT-F3N-Br/active layer/PNDIT-F3N-Br/Ag. The mobilities (μ) were determined by fitting the dark current to the model of a single carrier SCLC, described by the equation:

$$J = \frac{9}{8}\varepsilon_0\varepsilon_r\mu\frac{V^2}{d^3}$$

where J is the current, E is the effective electric field, ε_0 is the permittivity of free space, ε_r is the material relative permittivity, d is the thickness of the active layer, and V is the effective voltage. The effective voltage can be obtained by subtracting the built-in voltage (V_{bi}) and the voltage drop (V_s) from the substrate's series resistance from the applied voltage (V_{appl}), $V = V_{appl} - V_{bi} - V_s$. The mobility can be calculated from the slope of the $J^{1/2} \sim V$ curves.

The electrochemical behavior of a material was investigated using cyclic voltammetry (CHI 630A Electrochemical Analyzer) with a standard three-electrode electrochemical cell in a 0.1 M Bu_4NPF_6 solution in CH_3CN at room temperature under an atmosphere of nitrogen with a scanning rate of 0.1 V/s. A carbon plate working electrode, a Pt wire counter electrode, and an $Ag/AgNO_3$ (0.01 M in CH_3CN) reference electrode were used. The experiments were calibrated with the standard ferrocene/ferrocenium (Fc) redox system and the assumption that the energy level of Fc is 4.8 eV below vacuum.

The contact angle tests were performed on a Dataphysics OCA40 Micro surface contact angle analyzer. The surface energy of the polymers and acceptors was characterized and calculated by the contact angles of the two probe liquids (water and diiodomethane) using the Wu model:

$$\gamma_{water}(1 + \cos\theta_{water}) = \frac{4\gamma_{water}^{d}\gamma^{d}}{\gamma_{water}^{d} + \gamma^{d}} + \frac{4\gamma_{water}^{p}\gamma^{p}}{\gamma_{water}^{p} + \gamma^{p}} \quad (1)$$

$$\gamma_{oil}(1 + \cos\theta_{oil}) = \frac{4\gamma_{oil}^{d}\gamma^{d}}{\gamma_{oil}^{d} + \gamma^{d}} + \frac{4\gamma_{oil}^{p}\gamma^{p}}{\gamma_{oil}^{p} + \gamma^{p}}$$

$$\gamma = \gamma^{d} + \gamma^{p} \quad (2)$$

where γ is the total surface tension of acceptor and polymers; γ^d and γ^p are the dispersion and polar components of γ; γ_i is the total surface tension of the i material (i = water or diiodomethane); γ_i^d and γ_i^p are the dispersion and polar components of γ_i; and θ_i is the droplet contact angle of the i material on the acceptor and polymers films.

*Synthesis of compound **1***

In 50 mL two-necked flask, 2-(2-ethylhexyl)-thiophene (7.5 mmol, 1.47 g), bromobenzene (5 mmol, 785 mg), K_2CO_3 (7.5 mmol, 1.04 g), and palladium acetate (0.5 mmol, 1.2 mg) were dissolved in 20 mL ultra-dry *N*,*N*-dimethylacetamide. And then the solution was heated at 80 °C in the dark for 4 h, and run the TLC to confirm the end point of the reaction. The reaction solution was cooled to room temperature, quenched with water, extracted three times with ethyl acetate, washed with distilled water three times. The organic phase was collected, dried with anhydrous magnesium sulfate, filtered, spun to dry the solvent, and separated and purified by silica gel chromatography with petroleum ether as the eluent. A yellow liquid compound (817.3 mg, 60%) was obtained. ^{1}H NMR (400 MHz, $CDCl_3$) δ 7.60 – 7.51 (m, 2H), 7.34 (dd, J = 10.5, 4.8 Hz, 2H), 7.22 (dd, J = 10.4, 4.4 Hz, 1H), 7.12 (d, J = 3.5 Hz, 1H), 6.71 (d, J = 3.5 Hz, 1H), 2.75 (d, J = 6.8 Hz, 2H), 1.66 – 1.54 (m, 1H), 1.37 – 1.23 (m, 8H), 0.92 – 0.88 (m, 6H).

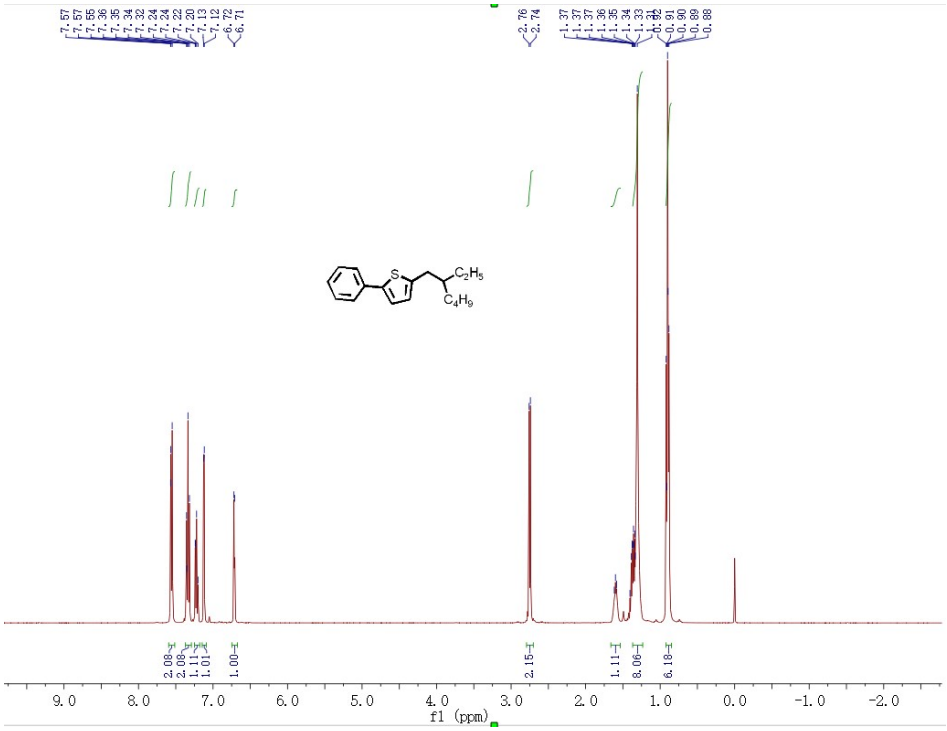

Fig. S1 ^{1}H NMR spectrum of compound **1**.

*Synthesis of compound **EP-BDD***

In 100 mL two-necked flask, 2,5-dibromo-3,4-thiophenedicarboxylic acid (3 mmol, 989.85 mg) was dissolved in 30 mL ultra-dry dichloromethane, and then 1 mL ultra-dry *N*,*N*-dimethylacetamide was added. Subsequently, oxalyl chloride (12 mmol, 1.53 g) was added dropwise into the reaction. The reaction was proceeded at room temperature for more than 12 hours. After removing the solvent, a yellow intermediate was obtained and directly used without further purification. The yellow

intermediate and compound **1** (3 mmol, 817.3 mg) were dissolved in 30 mL ultra-dry dichloromethane, and then aluminum chloride (12 mmol, 1.6 g) was added by three portions at 0 ℃. After that, the reaction was warmed to room temperature slowly and reacted overnight. The crude product was extracted with dichloromethane, washed with water, and dried with anhydrous magnesium sulfate. After removing the solvent, the product was purified by silica gel column chromatography with petroleum ether:dichloromethane (4:1) as the eluent. Compound **EP-BDD** was obtained as a yellow solid (1.14 g, 67%). ^{1}H NMR (500 MHz, $CDCl_3$) δ ppm: 7.60 (q, 2H), 7.44 (t, 3H), 3.4(m, 2H), 1.81 (m, 1H), 1.33 (m, 8H), 0.88 (m, 6H). ^{13}C NMR (101 MHz, $CDCl_3$) δ 175.58 (s), 174.16 (s), 157.39 (s), 150.40 (s), 134.64 (d, J = 14.7 Hz), 133.36 (s), 132.25 (s), 131.50 (s), 129.78 (s), 129.42 (s), 128.25 (s), 119.95 (s), 119.65 (s), 41.13 (s), 34.11 (s), 32.66 (s), 28.71 (s), 25.90 (s), 23.03 (s), 14.14 (s), 10.80 (s).

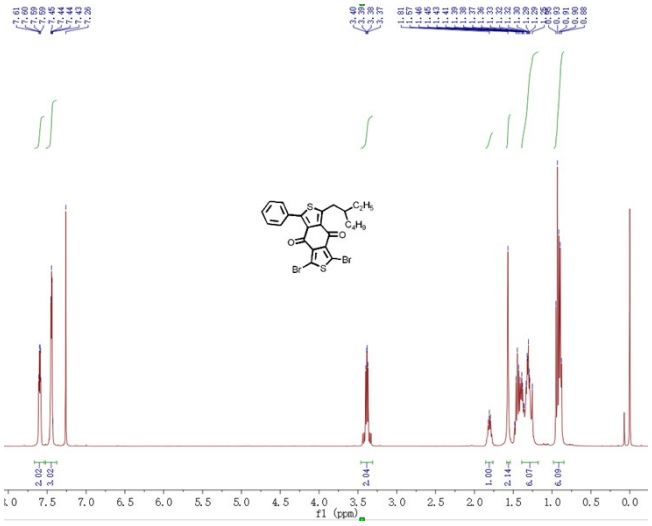

Fig. S2 ^{1}H NMR spectrum of EP-BDD.

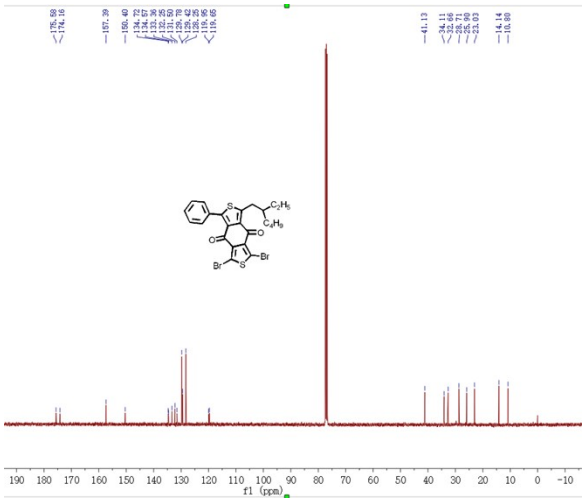

Fig. S3 ^{13}C NMR spectrum of EP-BDD.

*Synthesis of **EP-BDD-T***

In 50 mL two-necked flask, compound **EP-BDD** (2 mmol, 1.14 g), 2-tributylstannylthiophene (6 mmol, 2.24 g), and $Pd(PPh_3)_4$ (0.12 mmol, 138 mg) were dissolved in 20 mL ultra-dry *o*-xylene. And then the solution was heated at 110 °C overnight, and the reaction was monitored by TLC. After reaction completed, the reaction was cooled to room temperature slowly. The reaction was extracted three times with ethyl acetate, and the organic phase was washed with distilled water three times, and dried with anhydrous magnesium sulfate. After removing the organic solvent by rotary evaporation, the crude product was purified by silica gel chromatography with petroleum ether:dichloromethane (4:1) as the eluent, leading to a yellow solid (1.1 g, 95%). ^{1}H NMR (400 MHz, $CDCl_3$) δ 7.79 – 7.69 (m, 2H), 7.62 (dd, *J* = 6.6, 2.9 Hz, 2H), 7.51 (dd, *J* = 5.1, 0.8 Hz, 1H), 7.42 (dd, *J* = 7.9, 3.8 Hz, 4H), 7.10 (ddd, *J* = 26.5, 5.0, 3.8 Hz, 2H), 3.38 (d, *J* = 7.0 Hz, 2H), 2.16 – 1.90 (m, 1H), 1.91 – 1.72 (m, 2H), 1.45 – 1.31 (m, 6H), 0.92 (dt, *J* = 16.6, 7.2 Hz, 6H). ^{13}C NMR (101 MHz, $CDCl_3$) δ 155.80 (s), 132.92 – 132.31 (m), 130.69 (d, *J* = 13.3 Hz), 129.85 (s), 129.36 (d, *J* = 9.3 Hz), 129.06 (s), 128.14 (s), 127.29 (d, *J* = 7.8 Hz), 77.35 (s), 77.03 (s), 76.71 (s), 41.27 (s), 33.80 (s), 32.80 (s), 28.83 (s), 25.99 (s), 23.04 (s), 14.18 (s), 10.89 (s).

In 100 mL flask, the above yellow product (2 mmol, 1.1 g) was dissolved in chloroform (20 mL), and then NBS (4.2 mmol, 748 mg) was added into the solution at 0 ℃. The reaction turned to room temperature for overnight in the dark. After quenching the reaction with water, the solution was extracted three times with dichloromethane, and then washed with distilled water three times. The organic phase was collected, and dried with anhydrous magnesium sulfate. The solvent was removed by rotary evaporation. After purification by silica gel chromatography with petroleum ether:dichloromethane (4:1) as the eluent, the final product **EP-BDD-T** was obtained as orange-yellow solid (1.3 g, 90%). ^{1}H NMR (400 MHz, $CDCl_3$) δ 7.62 (dd, *J* = 6.5, 2.9 Hz, 2H), 7.55 – 7.32 (m, 5H), 7.04 (dd, *J* = 22.1, 4.0 Hz, 2H), 3.36 (qd, *J* = 15.0, 7.0 Hz, 2H), 1.87 – 1.71 (m, 1H), 1.49 – 1.23 (m, 8H), 0.93 (dt, *J* = 9.2, 7.2 Hz, 6H). ^{13}C NMR (101 MHz, $CDCl_3$) δ 177.64 (s), 176.39 (s), 156.30 (s), 149.40 (s), 141.68 (s), 134.50 (d, *J* = 13.1 Hz), 133.38 (s), 132.46 (s), 131.96 (s), 131.52 (s), 130.50 (d, *J* = 9.0 Hz), 129.86 (d, *J* = 7.9 Hz), 129.24 (s), 128.23 (s), 118.15 (d, *J* = 15.7 Hz), 41.22 (s), 33.85 (s), 32.87 (s), 28.91 (s), 26.02 (s), 23.07 (s), 14.25 (s), 10.87 (s).

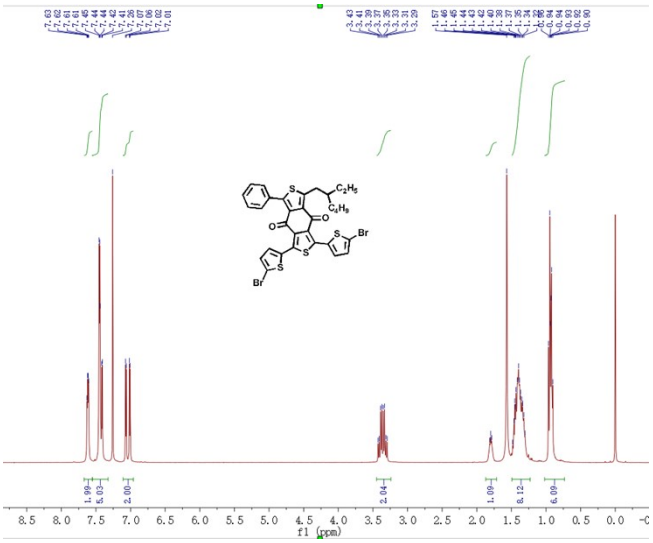

Fig. S4 ^{1}H NMR spectrum of EP-BDD-T.

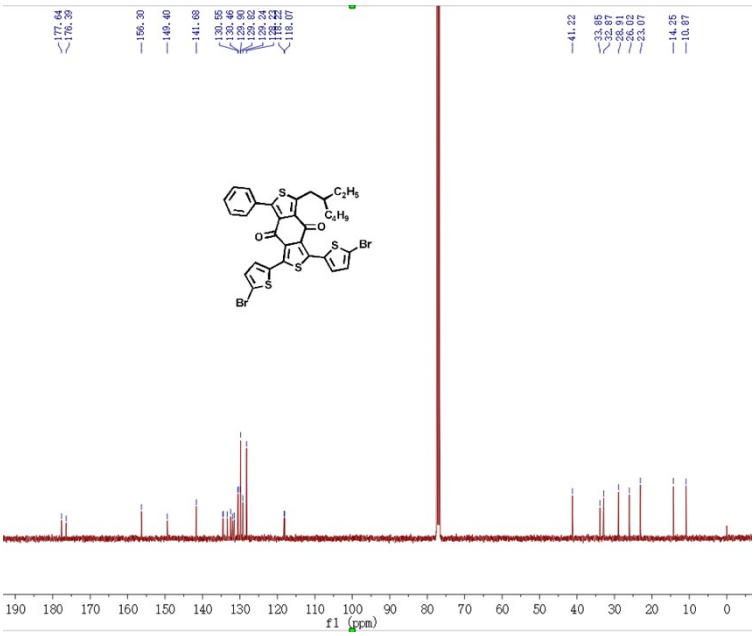

Fig. S5 ^{13}C NMR spectrum of EP-BDD-T.

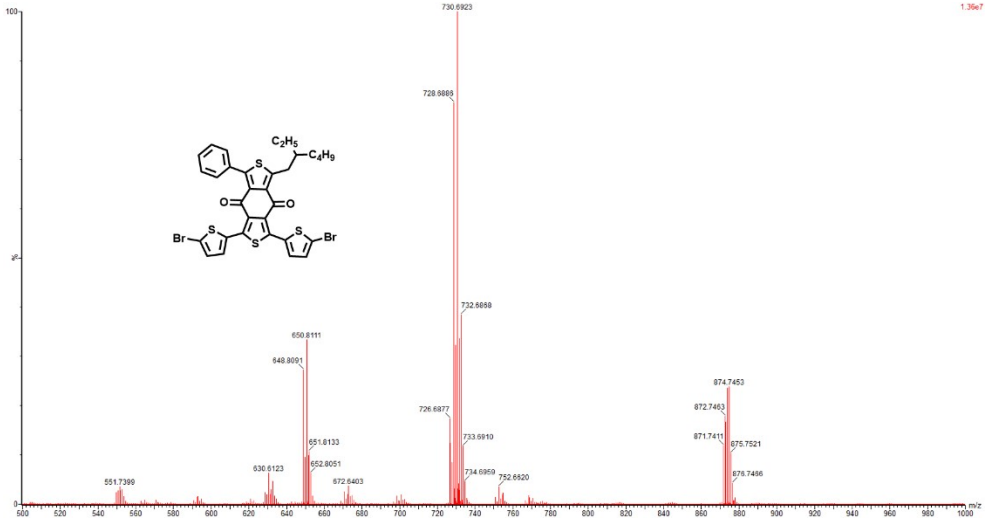

Fig. S6 MALDI-TOF mass spectrometry of EP-BDD-T

General procedure of polymerization

To a long Schlenk flask, F-BDT (1.0 eq.), EP-BDD-T (x eq.), and EH-BDD (1−x eq.) were dissolved in *o*-xylene (4 mL), and purged with argon for 30 min. Then, Pd $(PPh_3)_4$ (0.03 eq of F-BDT) was added and purged again with argon for 20 min. The reaction mixture was stirred at 120 °C for 72 h, and precipitated to methanol. The precipitate was then subjected to Soxhlet extraction with methanol, dichloromethane, and chloroform. Finally, the polymer was recovered as solid from the chloroform fraction by precipitation with methanol and dried under vacuum. The number-average molecular weights (M_n) and the polydispersity index (PDI) of polymers were measured by high temperature gel permeation chromatography (GPC) at 150 °C using 1,2,4-trichlorobenezene as eluent.

PM6 was prepared based on F-BDT (188.1 mg, 0.2 mmol, 1.0 eq.) and EH-BDD (153.3 mg, 0.2mmol, 1 eq), giving the product as black solid. Isolated yield = 82 %, M_n: 39.0 kDa, PDI: 2.31.

PhEH10 was prepared based on F-BDT (188.1 mg, 0.2 mmol, 1.0 eq.), EP-BDD-T (14.6 mg,0.02 mmol, 0.1eq.) and EH-BDD (139.8 mg,0.18mmol, 0.9 eq), giving the product as black solid. Isolated yield = 83 %, M_n: 30.5 kDa, PDI: 2.35.

PhEH20 was prepared based on F-BDT (188.1 mg, 0.2 mmol, 1.0 eq.), EP-BDD-T (29.2 mg,0.04 mmol, 0.2eq.) and EH-BDD (122.7 mg,0.16mmol, 0.8 eq), giving the product as black solid. Isolated yield = 80%, M_n: 30.2 kDa, PDI: 2.13.

PhEH50 was prepared based on F-BDT (188.1 mg, 0.2 mmol, 1.0 eq.), EP-BDD-T (73.1 mg,0.1 mmol, 0.5eq.) and EH-BDD (76.7 mg,0.1mmol, 0.5 eq), giving the product as black solid. Isolated yield = 80%, M_n: 37.8 kDa, PDI: 2.2.

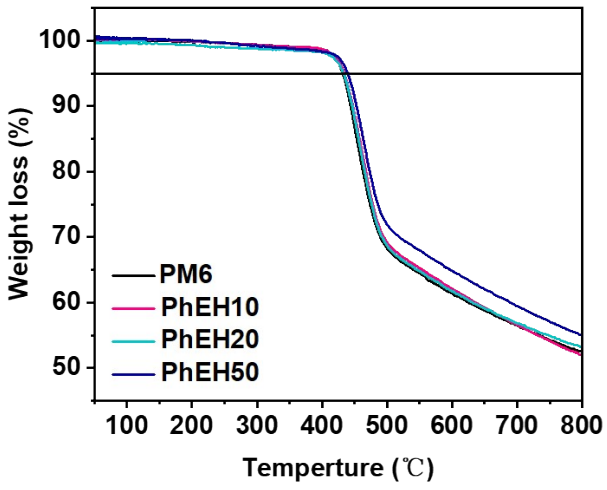

Fig. S7 TGA curves of the polymers.

Table S1. Summary of the optical and electrochemical properties of polymers

Polymer	λ_{sol} (nm)	λ_{film} (nm)	λ_{onset} (nm)	T_d (°C)	E_g [a] (eV)	HOMO [b] (eV)	LUMO [c] (eV)
PM6	614	616	682	431	1.81	−5.51	−3.70
PhEH10	617	622	695	434	1.78	−5.51	−3.73
PhEH20	620	622	688	435	1.80	−5.50	−3.70
PhEH50	616	621	699	439	1.77	−5.47	−3.70

[a] Calculated from the empirical equation $E_g = 1240/\lambda_{onset}$.

[b] Estimated from the cyclic voltammetry curve.

[c] Calculated from $E_{LUMO} = E_{HOMO} + E_g$.

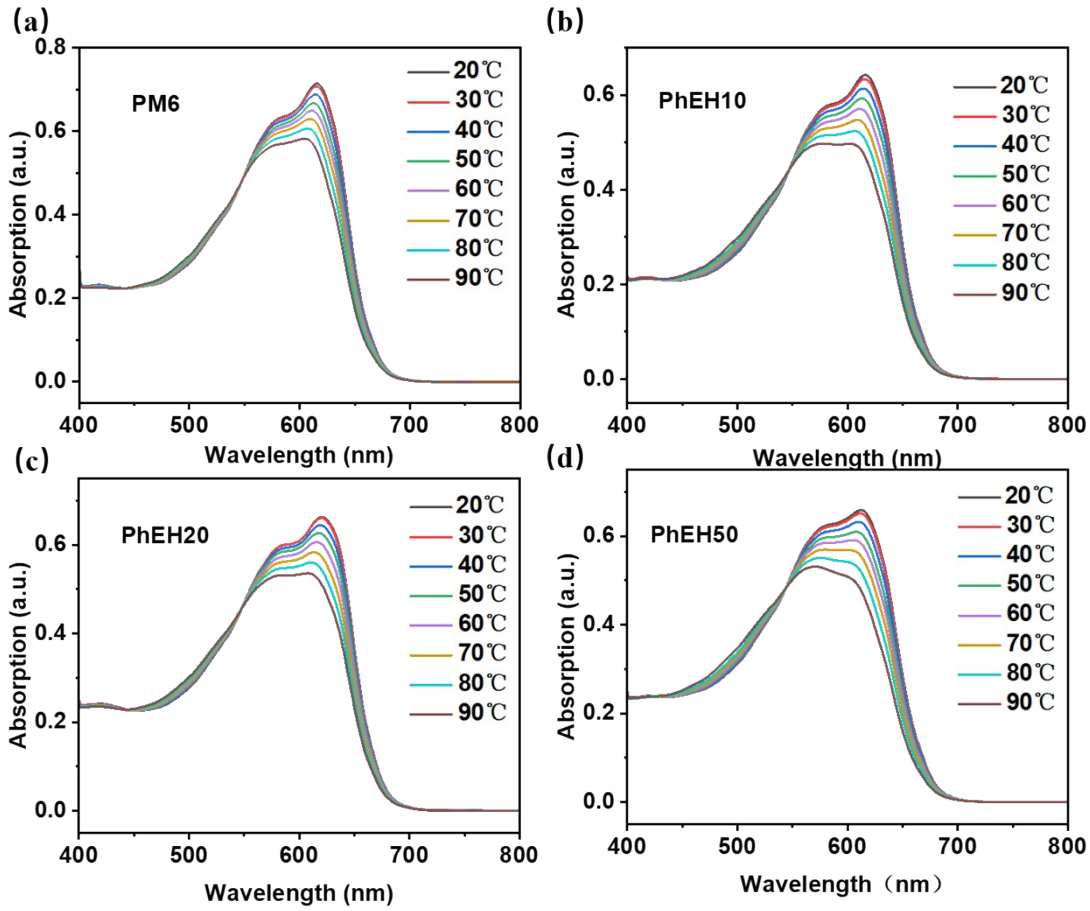

Fig. S8 Temperature dependent UV-Vis absorption spectra of chlorobenzene solution for (a) PM6, (b) PhEH10, (c) PhEH20, and (d) PhEH50.

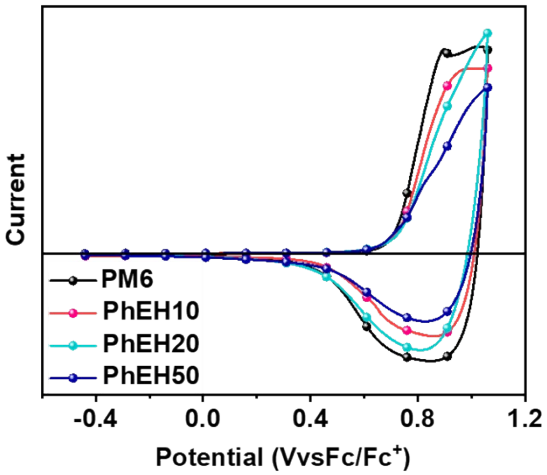

Fig. S9 CV curves of the polymers.

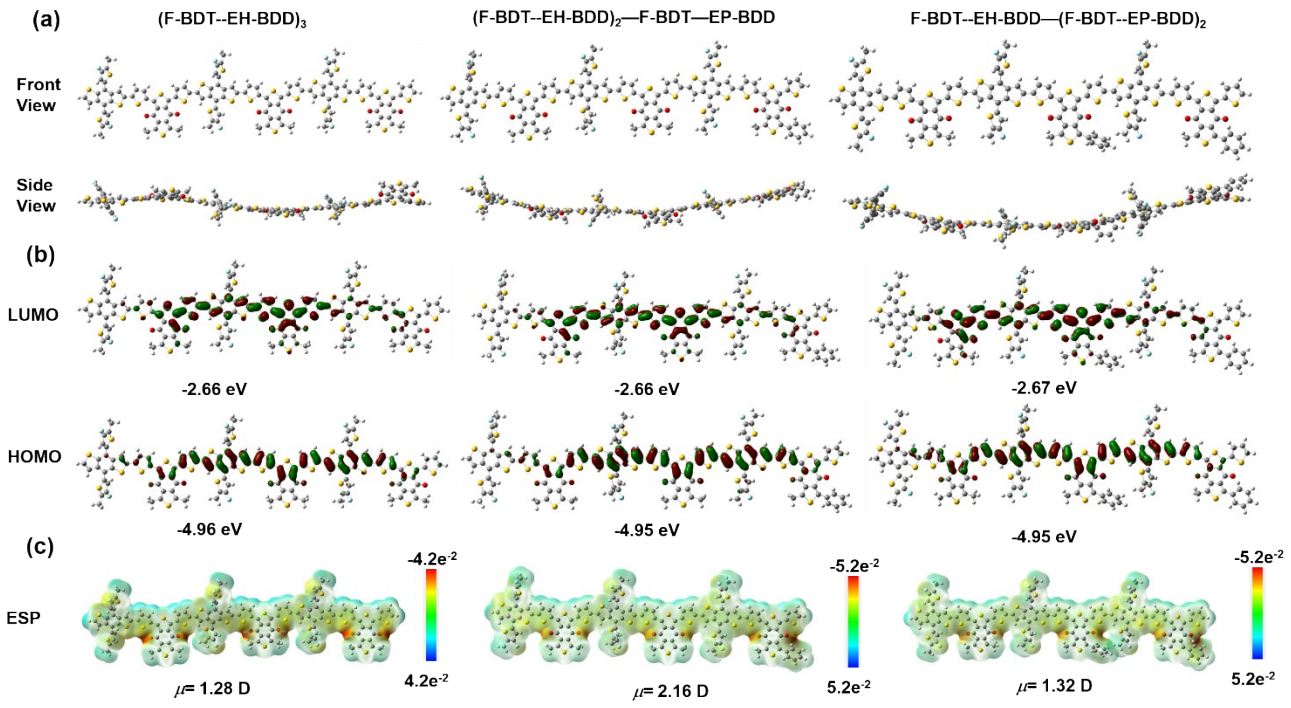

Fig. S10 (a) Simulated molecular geometries of the trimer by DFT calculations; (b) Calculated HOMO and LUMO energy levels; (c) the molecular electrostatic potential (ESP) distributions.

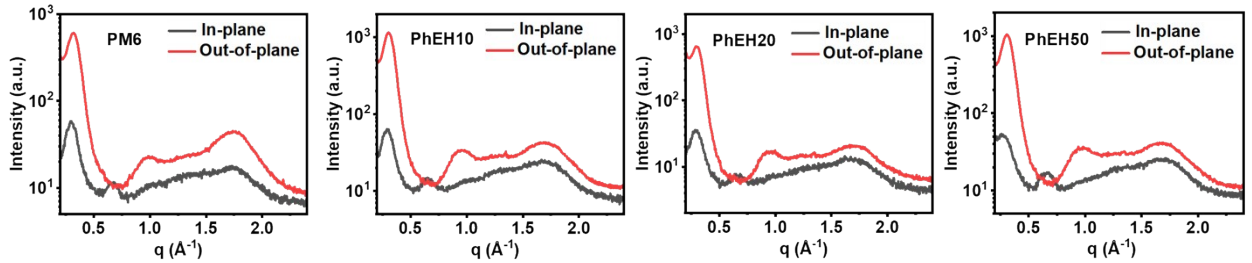

Fig. S11 GIWAXS corresponding line-cut profiles of pristine films of (a) PM6, (b) PhEH10, (c) PhEH20, and (d) PhEH50.

Table S2. Derived GIWAXS parameters of the pristine films.

Samples	In-plane			Out-of-plane		
	lamellar stacking (100)			π-π stacking (010)		
	q (Å^{-1})	d-spacing (Å)	CCL (Å)	q (Å^{-1})	d-spacing (Å)	CCL (Å)
PM6	0.301	20.87	108.75	1.73	3.63	26.77
PhEH10	0.291	21.59	161.11	1.68	3.74	56.27
PhEH20	0.287	21.89	149.60	1.64	3.83	48.00

PhEH50	0.263	23.89	68.13	1.66	3.79	54.42

Table S3. Face-on/(Face on + Edge-on) ratio of pristine polymers for lamellar stacking and π–π stacking diffraction.

Samples	Face-on/(Face on + Edge-on) ratio	
	(100) Lamellar stacking	(010) π-π stacking
PM6	0.1165	0.9332
PhEH10	0.1132	0.8942
PhEH20	0.0870	0.8578
PhEH50	0.0850	0.7521

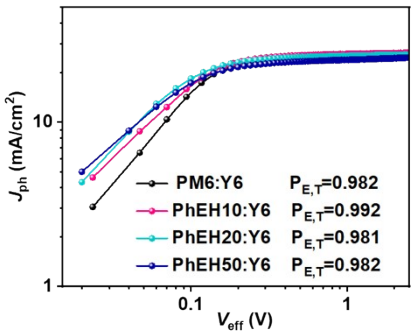

Fig. S12 Photocurrent density (J_{ph}) versus effective voltage (V_{eff}) characteristics

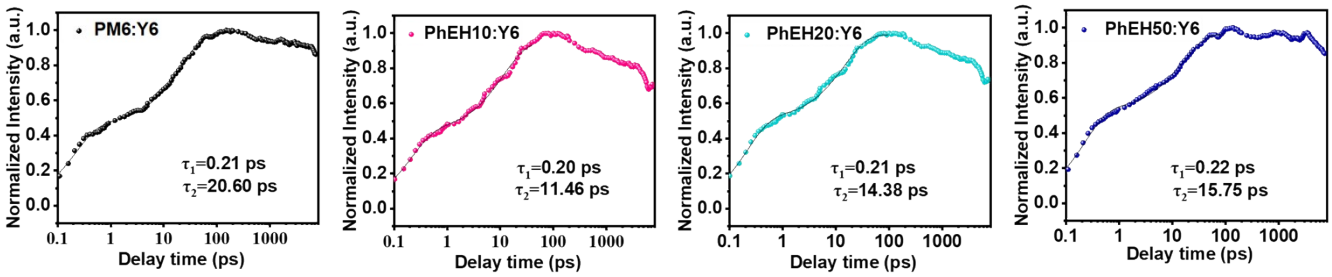

Fig. S13 Kinetic traces of the terpolymer donors GSB probing at 630 nm for the blend films.

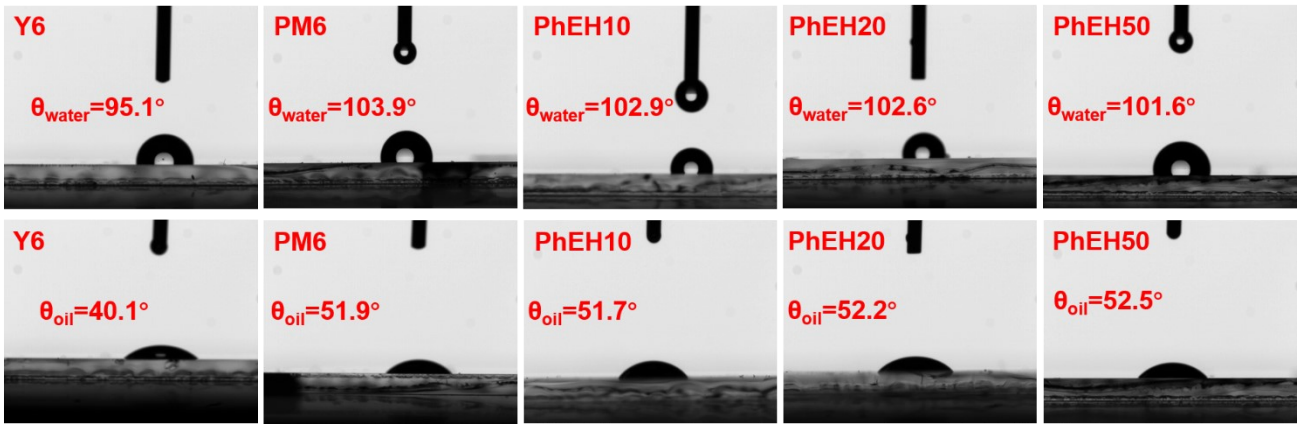

Fig. S14 Views of surface contact measurements for the polymer films using water and diiodine methane.

Table S4. The contact angles and surface energy parameters of the films.

Polymer	Contact angle		Dispersion component γ^d [mN/m]	Polar component γ^p [mN/m]	Surface free energy γ [mN/m]	$\chi_{donor,acceptor}$
	θ_{water}	θ_{oil}				
Y6	95.1	40.1	37.40	2.98	40.39	--
PM6	103.9	51.9	34.43	0.484	34.92	0.19K
PhEH10	102.9	51.7	33.82	0.896	34.72	0.21K
PhEH20	102.6	52.2	33.32	1.073	34.40	0.24K
PhEH50	101.6	52.5	32.67	1.509	34.18	0.26K

Table S5. Face-on/(Face on + Edge-on) ratio of blend films for lamellar stacking and π–π stacking crystallites.

Samples	Face-on/(Face on + Edge-on) ratio	
	(100) Lamellar stacking	(010) π-π stacking
PM6:Y6	0.5349	0.9871
PhEH10:Y6	0.5197	0.9864
PhEH20:Y6	0.5177	0.9863
PhEH50:Y6	0.5031	0.9750

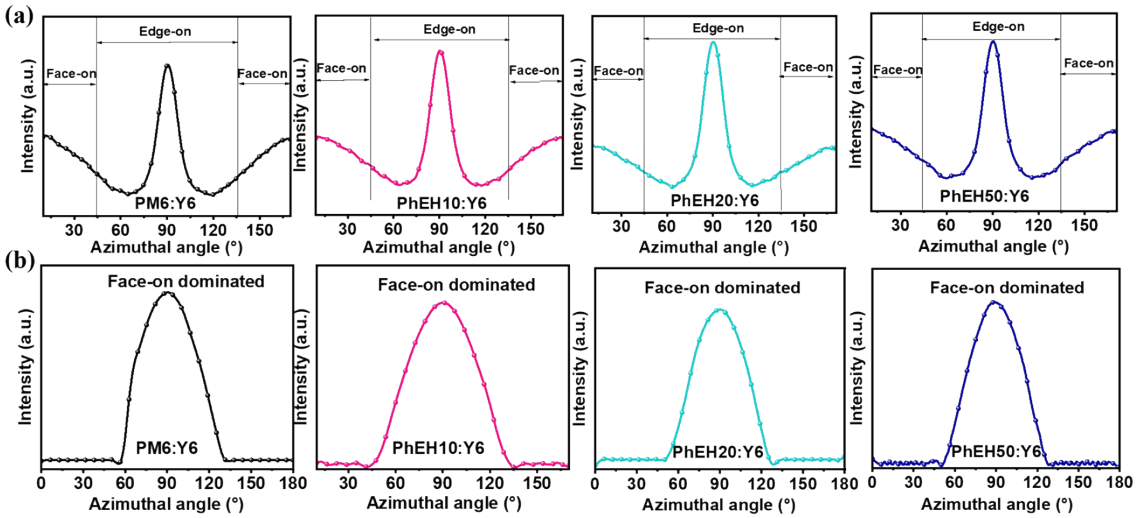

Fig. S15 Azimuthal pole figures of the blend films along with (a) lamellar stacking and (b) π–π stacking diffraction.

Table S6. Derived GIWAXS parameters of the blend films.

Samples	In-plane			Out-of-plane		
	lamellar stacking (100)			π-π stacking (010)		
	q (Å^{-1})	d-spacing (Å)	CCL (Å)	q (Å^{-1})	d-spacing (Å)	CCL (Å)
PM6:Y6	0.291	21.59	110.45	1.73	3.63	37.01
PhEH10:Y6	0.301	20.87	111.76	1.74	3.61	44.88
PhEH20:Y6	0.287	21.89	105.92	1.72	3.65	42.52
PhEH50:Y6	0.291	21.59	105.86	1.72	3.65	41.89

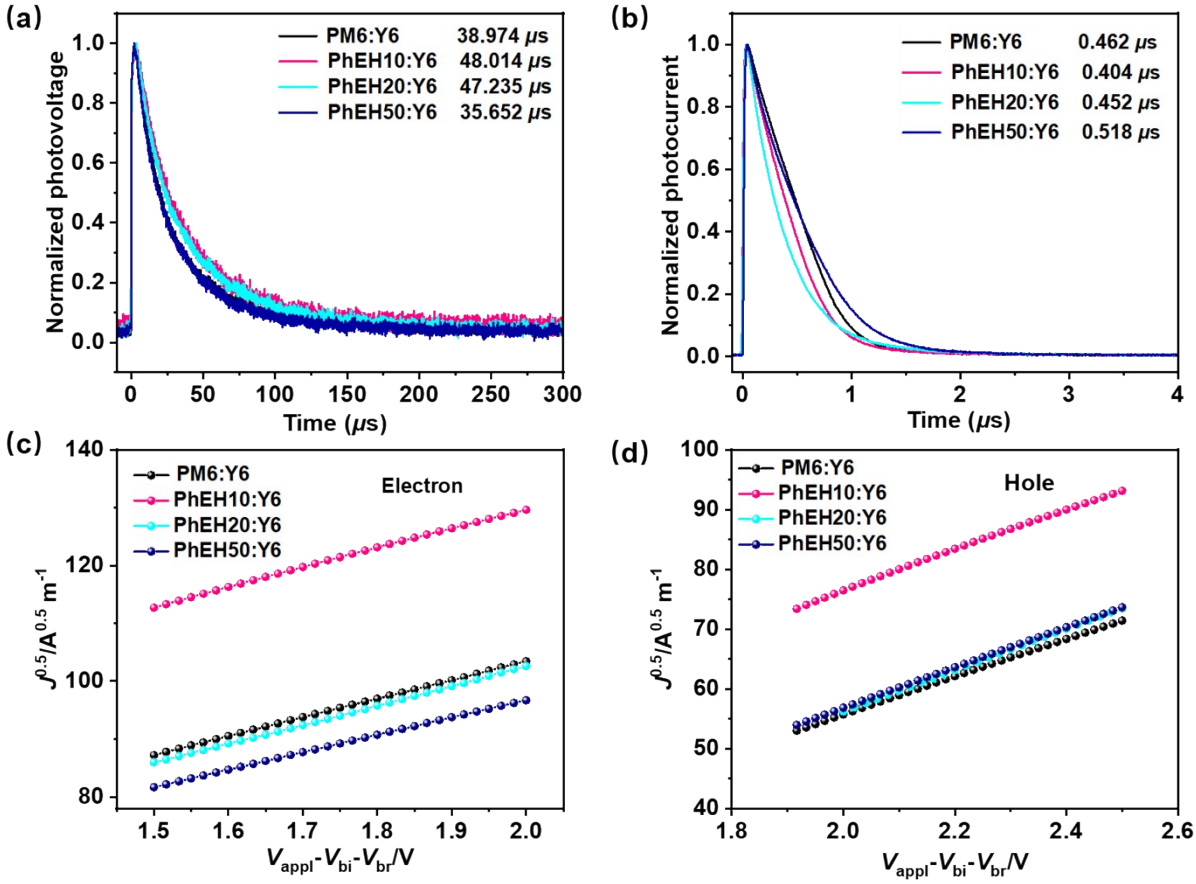

Fig. S16 (a) TPV, (b) TPC, (c) Electron mobilities, (d) Hole mobilities for the PM6- , PhEH10-, Ph EH20-, and PhEH50-based OSCs.

Table S7. Charge mobilities of the blend films

Active layer	Hole mobility ($cm^2\ V^{-1}\ s^{-1}$)	Electron mobility ($cm^2\ V^{-1}\ s^{-1}$)	μ_h/μ_e
PM6:Y6	3.34×10^{-4}	2.88×10^{-4}	1.16
PhEH10:Y6	4.02×10^{-4}	3.95×10^{-4}	1.02
PhEH20:Y6	3.84×10^{-4}	3.37×10^{-4}	1.14
PhEH50:Y6	3.83×10^{-4}	3.36×10^{-4}	1.14

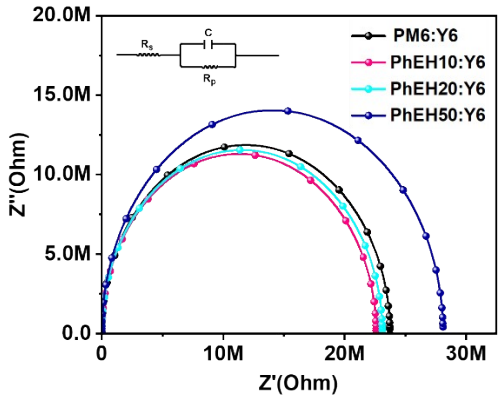

Fig. S17 Nyquist plot of the solar devices and the equivalent-circuit model employed for EIS fitting. Active layer=PM6:Y6, PhEH10:Y6, PhEH20:Y6, PhEH50:Y6.

Table S8. Electrochemical impedance spectrum test data of devices

Active layer	R_P (Ω)
PM6:Y6	2.37×10^7
PhEH10:Y6	2.26×10^7
PhEH20:Y6	2.31×10^7
PhEH50:Y6	2.81×10^7

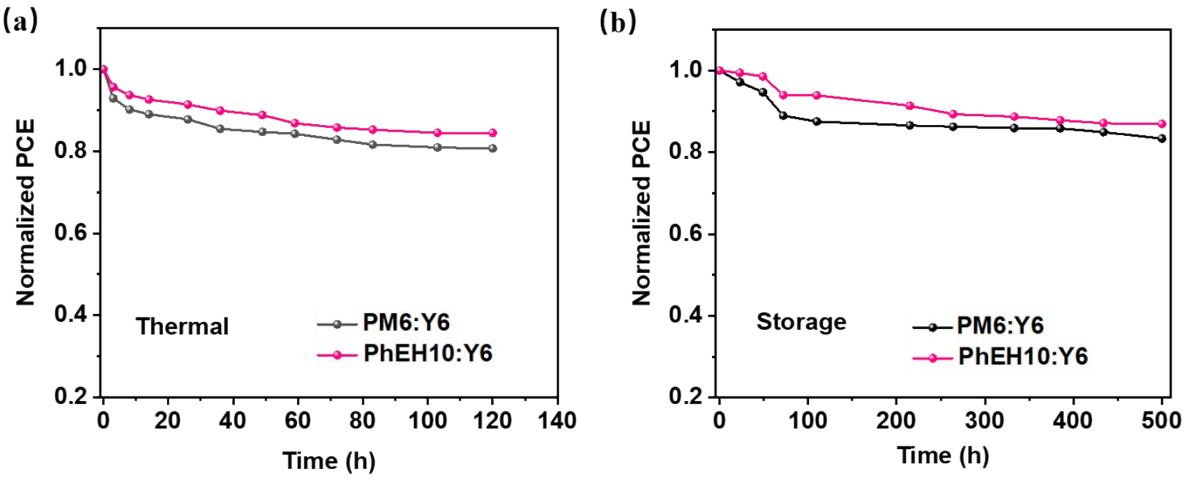

Fig. S18 (a) thermal stability, and (b) storage stability in air for the PM6- and PhEH10-based OSCs.

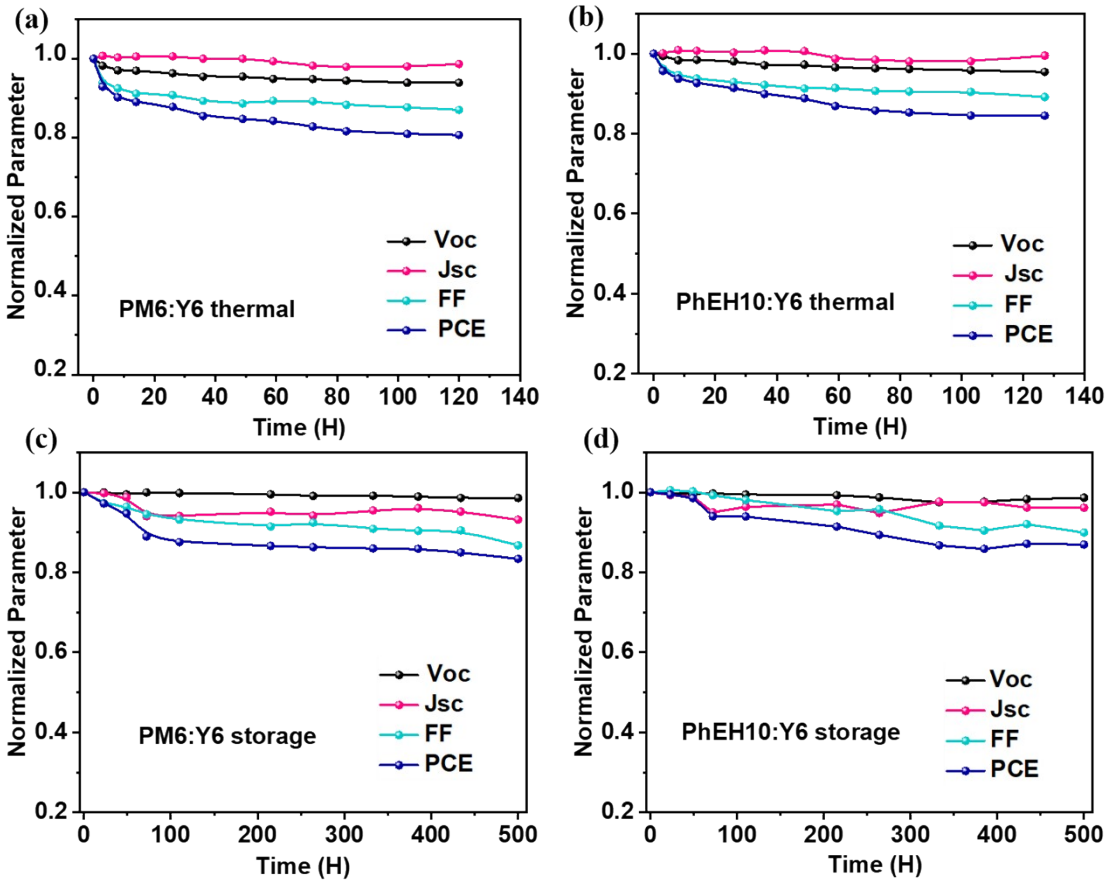

Fig. S19 Variation of relevant performance parameters of (a) PM6- and (b) PhEH10-based devices upon thermal stress. Variation of relevant performance parameters of (c) PM6- and (d) PhEH10-based devices in open air storage.

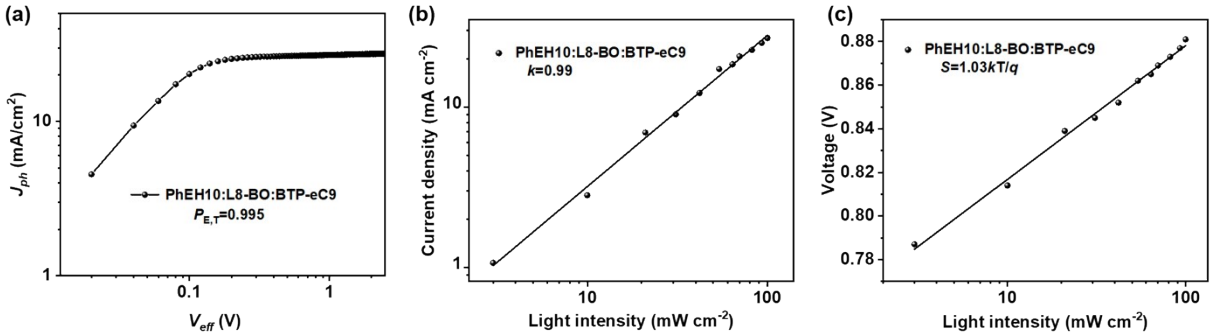

Fig. S20 (a) Photocurrent density (J_{ph}) versus effective voltage (V_{eff}) characteristics, and light intensity dependence of (b) J_{sc} and (c) V_{oc} for PhEH10:L8-BO:BTP-eC9 based devices.

Table S9. Summary of photovoltaic parameters of the terpolymer-based OSCs.

Active layer	Category	V_{oc} [V]	J_{sc} [mA cm^{-2}]	FF [%]	PCE [%]	Ref.
PMZ-10: Y6	D-A1-D-A2	0.834	27.96	78.20	18.23	1
SZ4:N3		0.848	26.00	77.40	17.10	2
PM6-Tz20:Y6		0.860	27.30	75.00	17.60	3
PM6-C10:Y7		0.860	26.97	74.00	17.00	4
PW1: BTP-ec9-4F		0.860	26.97	70.45	16.23	5
PL1: BTP-eC9-4F		0.876	27.11	76.40	18.14	6
PM1:Y6		0.870	25.90	78.00	17.60	7
PM6-CNBT-10: L8-BO		0.902	25.77	77.50	18.01	8
PM6-TTO-10: BTP-eC9		0.860	26.80	79.97	18.37	9
PMZ2:Y6		0.854	26.90	77.20	17.80	10
H9:Y6		0.890	26.68	77.89	18.50	11
OPz1:Y6		0.871	25.34	73.7	16.28	12
OPz11:Y6		0.865	27.02	78.71	18.42	13
PF1:Y6		0.870	26.30	76.00	17.30	14
PM6-BNBP-4: L8-BO		0.909	26.65	78.97	19.13	15
DL1:Y6		0.869	27.82	78.94	19.10	16
PBDT-TZ-BDD-1/19: ITIC		0.93	17.56	67.48	11.02	17
T1: ITIC		0.952	16.80	71.91	11.50	18
PBDB-TAZ20: ITIC		0.865	19.03	73.5	12.34	19
PBN-Cl-B80: IT-4F		0.891	21.85	72.1	14.05	20
TP-H: Y6		0.851	26.78	73.53	16.76	21
PBTPBD-50: IT-4F		0.82	21.99	75.67	13.64	22
PQB2: PY-IT		0.942	24.2	0.795	18.1	23
P1-co-25%P2: PYFT		0.83	23.51	73.09	14.67	24
T1(E-T): IT-4F		0.899	21.5	0.78	15.1	25
PBDB-TF-TT10: Y6		0.80	25.1	0.66	13.3	26
PBDB-TF-T10: Y6		0.84	27.9	0.70	16.4	26
S3(Cl-T): Y6		0.890	25.26	71.69	16.12	27
S1: Y6		0.877	25.4	73.7	16.42	28
PFBCNT20: Y6-BO		0.84	26.3	73.9	16.3	29

P5TCN-F25: Y6		0.79	27.13	77.1	16.6	30
Pt10: Y6		0.81	26.45	76.3	16.35	31
PTB7-Th-bdq5: IEICO-4F		0.736	21.83	64	10.27	32
PM6Ir1: Y6		0.848	26.16	75.33	16.71	33
PFBT4T-T20: Y14		0.79	26.56	74.34	15.60	34
TBD:IT-4F	D1-A-D2-A	0.892	20.8	76.8	14.2	35
J52-TBF50: ITIC		0.790	17.93	72.8	10.32	36
TBFCl50-FTAZ: ITIC		0.876	18.45	73.8	11.94	36
TBFCl50-BDD: ITIC		0.961	18.17	71.3	12.46	36
PTPTI-T70: m-ITIC		0.93	17.12	69.26	11.02	37
PBDB-TT5: m-ITIC		0.913	17.53	69.79	11.17	38
PM20Si:Y6		0.80	26.92	70.44	15.17	39
PTQ10 90:10: Y6		0.81	25.5	68	13.8	40
PL-1: Y6	D-A-D'-A	0.820	25.57	78.10	16.37	41
D18-20%Cl: Y6		0.861	27.20	78.06	18.28	42
PM6-Si30: PM6:C9		0.870	26.90	78.04	18.27	43
PCE10-BDT2F-0.7: Y6		0.746	26.17	68.95	13.46	44
PB55: ITCPTC		0.93	17.0	74.8	12.1	45
PBTA-PS-F: ITIC		0.97	18.46	75.29	13.48	46
PFBT4T-C5Si-25%: PC71BM		0.76	19.08	74.12	11.09	47
PTBSi25: IEICO-4F		0.71	25.57	69.24	12.61	48
PF7:Y6-BO-4Cl		0.86	26.95	79	18.31	49
PBDTBD-50: IT-4F		0.80	17.16	73.1	10.03	50
PDCBT-Cl-Si5: ITIC-Th1		0.93	18.70	70.1	12.67	51
PQSi05: IT-4F	D-A-D-A'	0.911	21.42	69.48	13.56	52
PQSi705:m-TEH		0.887	26.72	76.55	18.00	53
PhEH10:Y6		0.841	26.8	75.8	17.0	This work
PhEH10:L8-BO		0.883	25.8	80.7	18.5	
PhEH10:L8-BO: BTP-eC9		0.878	26.97	80.39	19.03	

Reference:

1. L. Zhou, L. Meng, J. Zhang, C. Zhu, S. Qin, I. Angunawela, Y. Wan, H. Ade and Y. Li, *Adv.*

Funct. Mater., 2022, **32**, 2109271.

2. J. Liang, M. Pan, G. Chai, Z. Peng, J. Zhang, S. Luo, Q. Han, Y. Chen, A. Shang, F. Bai, Y. Xu, H. Yu, J. Y. L. Lai, Q. Chen, M. Zhang, H. Ade and H. Yan, *Adv. Mater.*, 2020, **32**, 2003500.
3. X. Guo, Q. Fan, J. Wu, G. Li, Z. Peng, W. Su, J. Lin, L. Hou, Y. Qin, H. Ade, L. Ye, M. Zhang and Y. Li, *Angew. Chem. Int. Ed.*, 2021, **60**, 2322-2329.
4. J.-W. Lee, D. Jeong, D. J. Kim, T. N.-L. Phan, J. S. Park, T.-S. Kim and B. J. Kim, *Energy Environ. Sci.*, 2021, **14**, 4067-4076.
5. H. Wang, H. Lu, Y.-N. Chen, A. Zhang, Y. Liu, D. Li, Y. Liu, X. Xu and Z. Bo, *Adv.Energy Mater.*, 2022, **12**, 2104028.
6. H. Lu, H. Wang, G. Ran, S. Li, J. Zhang, Y. Liu, W. Zhang, X. Xu and Z. Bo, *Adv. Funct. Mater.*, 2022, **32**, 2203193.
7. J. Wu, G. Li, J. Fang, X. Guo, L. Zhu, B. Guo, Y. Wang, G. Zhang, L. Arunagiri, F. Liu, H. Yan, M. Zhang and Y. Li, *Nat. Commun.*, 2020, **11**, 4612.
8. J. Shao, C. Liao, X. Xu, M. Deng, L. Yu, R. Li and Q. Peng, *Chem. Mater.*, 2022, **34**, 7971-7981.
9. F. Cheng, Y. Cui, F. Ding, Z. Chen, Q. Xie, X. Xia, P. Zhu, X. Lu, H. Zhu, X. Liao and Y. Chen, *Adv. Mater.*, 2023, **35**, 2300820.
10. J. Wu, X. Guo, M. Xiong, X. Xia, Q. Li, J. Fang, X. Yan, Q. Liu, X. Lu, E. Wang, D. Yu and M. Zhang, *Chem. Eng. J.*, 2022, **446**, 137424.
11. B. Huang, X. Deng, H. Jin, K. Liu, S. Chen, Z. Ma, J. Oh, C. Yang, J. Liu and L. Chen, *J. Mater. Chem. A*, 2022, **10**, 18714-18722.

12. Z. Liao, K. Yang, L. Hou, J. Li, J. Lv, R. Singh, M. Kumar, Q. Chen, X. Dong, T. Xu, C. Hu, T. Duan, Z. Kan, S. Lu and Z. Xiao, *Macromolecules*, 2020, **53**, 9034-9042.

13. Z. Liao, D. Hu, H. Tang, P. Huang, R. Singh, S. Chung, K. Cho, M. Kumar, L. Hou, Q. Chen, W. Yu, H. Chen, K. Yang, Z. Kan, F. Liu, Z. Xiao, G. Li and S. Lu, *J. Mater. Chem. A*, 2022, **10**, 7878-7887.

14. Q. Guo, J. Lin, X. Dong, L. Zhu, X. Guo, F. Liu and M. Zhang, *Chem. Eng. J.*, 2022, **431**, 134117.

15. S. Hao, X. Xu, L. Yu, S. Peng, J. Xia, Y. Xie, C. Duan, H. Wu, R. Li and Q. Peng, *Adv. Mater.*, 2023, **35**, 2301732.

16. D. He, J. Zhou, Y. Zhu, Y. Li, K. Wang, J. Li, J. Zhang, B. Li, Y. Lin, Y. He, C. Wang and F. Zhao, *Adv. Mater.*, 2023, **n/a**, 2308909.

17. H. Lei, B. Huang, L. Chen, S. Chen, G. Xu, S. Huang, Y. Tan, C. Yang and Y. Chen, *Sol. RRL*, 2019, **3**, 1900122.

18. J. Li, Z. Liang, X. Li, H. Li, Y. Wang, J. Qin, J. Tong, L. Yan, X. Bao and Y. Xia, *ACS Appl. Mater. Interfaces*, 2020, **12**, 8475-8484.

19. Y. Zhang, Y. Shao, Z. Wei, L. Zhang, Y. Hu, L. Chen, S. Chen, Z. Yuan and Y. Chen, *ACS Appl. Mater. Interfaces*, 2020, **12**, 20741-20749.

20. H. Yang, Y. Wu, Y. Dong, C. Cui and Y. Li, *ACS Appl. Mater. Interfaces*, 2019, **11**, 40339-40346.

21. L. Xu, W. Tao, M. Guan, X. Yang, M. Huang, H. Chen, J. Zhang, B. Zhao and S. Tan, *ACS Appl.Energy Mater.*, 2021, **4**, 11624-11633.

22. H. Jung, G. Yu, J. Kim, H. Bae, M. Kim, K. Kim, B. Kim and Y. Lee, *Sol. RRL*, 2021, **5**,

2100513.

23. T. Zhang, Y. Xu, H. Yao, J. Zhang, P. Bi, Z. Chen, J. Wang, Y. Cui, L. Ma, K. Xian, Z. Li, X. Hao, Z. Wei and J. Hou, *Energy Environ. Sci.*, 2023, **16**, 1581-1589.

24. Z. Li, Y. Liang, X. Qian, L. Ying and Y. Cao, *Chem. Eng. J.*, 2022, **439**, 135491.

25. Y. Cui, H. Yao, L. Hong, T. Zhang, Y. Xu, K. Xian, B. Gao, J. Qin, J. Zhang, Z. Wei and J. Hou, *Adv. Mater.*, 2019, **31**, 1808356.

26. Y. Xu, Q. Ji, L. Yin, N. Zhang, T. Liu, N. Li, X. He, G. Wen, W. Zhang, L. Yu, P. Murto and X. Xu, *ACS Appl. Mater. Interfaces*, 2021, **13**, 23993-24004.

27. Q. An, J. Wang, X. Ma, J. Gao, Z. Hu, B. Liu, H. Sun, X. Guo, X. Zhang and F. Zhang, *Energy Environ. Sci.*, 2020, **13**, 5039-5047.

28. H. Sun, T. Liu, J. Yu, T.-K. Lau, G. Zhang, Y. Zhang, M. Su, Y. Tang, R. Ma, B. Liu, J. Liang, K. Feng, X. Lu, X. Guo, F. Gao and H. Yan, *Energy Environ. Sci.*, 2019, **12**, 3328-3337.

29. Y. Zhang, L. Pan, Z. Peng, W. Deng, B. Zhang, X. Yuan, Z. Chen, L. Ye, H. Wu, X. Gao, Z. Liu, C. Duan, F. Huang and Y. Cao, *J. Mater. Chem. A*, 2021, **9**, 13522-13530.

30. X. Yuan, Y. Zhao, D. Xie, L. Pan, X. Liu, C. Duan, F. Huang and Y. Cao, *Joule*, 2022, **6**, 647-661.

31. X. Xu, K. Feng, Z. Bi, W. Ma, G. Zhang and Q. Peng, *Adv. Mater.*, 2019, **31**, 1901872.

32. X. Gao, R. Yu, X. Song, X. Tao, H. Wang, M. Zhu, Y. Wu, Y. He and Y. Tao, *J. Mater. Chem. C*, 2021, **9**, 7035-7045.

33. M. Zhang, X. Ma, H. Zhang, L. Zhu, L. Xu, F. Zhang, C.-S. Tsang, L. Y. S. Lee, H. Y. Woo, Z. He and W.-Y. Wong, *Chem. Eng. J.*, 2022, **430**, 132832.

34. J. Liang, S. Lei, L. Zhang, F. Pan, M. Luo, H. Liu, Z. Zhang, D. Yuan and J. Chen, *ACS Appl.Energy Mater.*, 2022, **5**, 11866-11873.

35. X. Wang, J. Han, D. Huang, J. Wang, Y. Xie, Z. Liu, Y. Li, C. Yang, Y. Zhang, Z. He, X. Bao and R. Yang, *ACS Appl. Mater. Interfaces*, 2020, **12**, 20393-20403.

36. X. Wang, K. Dou, B. Shahid, Z. Liu, Y. Li, M. Sun, N. Zheng, X. Bao and R. Yang, *Chem. Mater.*, 2019, **31**, 6163-6173.

37. S. Chen, H. J. Cho, J. Lee, Y. Yang, Z.-G. Zhang, Y. Li and C. Yang, *Adv.Energy Mater.*, 2017, **7**, 1701125.

38. M. Jeong, S. Chen, S. M. Lee, Z. Wang, Y. Yang, Z.-G. Zhang, C. Zhang, M. Xiao, Y. Li and C. Yang, *Adv.Energy Mater.*, 2018, **8**, 1702166.

39. W. Xu, M. Zhang, J. Xiao, M. Zeng, L. Ye, C. Weng, B. Zhao, J. Zhang and S. Tan, *Polym.Chem.*, 2020, **11**, 6178-6186.

40. A. L. Jones, C. H. Y. Ho, S. A. Schneider, J. Zhang, Y. Pei, J. Wang, X. Zhan, S. R. Marder, M. F. Toney, F. So, G. N. Manjunatha Reddy and J. R. Reynolds, *Chem. Mater.*, 2022, **34**, 6853-6867.

41. X. Li, R. Ma, T. Liu, Y. Xiao, G. Chai, X. Lu, H. Yan and Y. Li, *Sci. China Chem.*, 2020, **63**, 1256-1261.

42. H.-R. Bai, Q. An, H.-F. Zhi, M. Jiang, A. Mahmood, L. Yan, M.-Q. Liu, Y.-Q. Liu, Y. Wang and J.-L. Wang, *ACS Energy Lett.*, 2022, **7**, 3045-3057.

43. W. Peng, Y. Lin, S. Y. Jeong, Z. Genene, A. Magomedov, H. Y. Woo, C. Chen, W. Wahyudi, Q. Tao, J. Deng, Y. Han, V. Getautis, W. Zhu, T. D. Anthopoulos and E. Wang, *Nano Energy*, 2022, **92**, 106681.

44. X. Huang, L. Zhang, Y. Cheng, J. Oh, C. Li, B. Huang, L. Zhao, J. Deng, Y. Zhang, Z. Liu, F. Wu, X. Hu, C. Yang, L. Chen and Y. Chen, *Adv. Funct. Mater.*, 2022, **32**, 2108634.

45. L. Huo, X. Xue, T. Liu, W. Xiong, F. Qi, B. Fan, D. Xie, F. Liu, C. Yang and Y. Sun, *Chem. Mater.*, 2018, **30**, 3294-3300.

46. X. Li, Z. Liang, H. Wang, S. Qiao, Z. Liu, H. Jiang, W. Chen and R. Yang, *J. Mater. Chem. A*, 2020, **8**, 1360-1367.

47. X. Liu, L. Nian, K. Gao, L. Zhang, L. Qing, Z. Wang, L. Ying, Z. Xie, Y. Ma, Y. Cao, F. Liu and J. Chen, *J. Mater. Chem. A*, 2017, **5**, 17619-17631.

48. Q. Wang, Z. Hu, Z. Wu, Y. Lin, L. Zhang, L. Liu, Y. Ma, Y. Cao and J. Chen, *ACS Appl. Mater. Interfaces*, 2020, **12**, 4659-4672.

49. H. Bin, J. Li, A. Caiazzo, M. M. Wienk, Y. Li and R. A. J. Janssen, *ChemSusChem*, 2023, **16**, e202300006.

50. H. Jung, G. Yu, S. Jang, I. Hwang, B. Kim, B. Kim and Y. Lee, *Org. Electron.*, 2020, **86**, 105929.

51. Q. Wang, M. Li, Z. Peng, N. Kirby, Y. Deng, L. Ye and Y. Geng, *Sci. China Chem.*, 2021, **64**, 478-487.

52. D. Yuan, F. Pan, L. Zhang, H. Jiang, M. Chen, W. Tang, G. Qin, Y. Cao and J. Chen, *Sol. RRL*, 2020, **4**, 2000062.

53. H. Liu, D. Yuan, H. Jiang, S. Li, L. Zhang and J. Chen, *Energy Environ. Sci.*, 2023, **16**, 3474-3485.